Cumulus Ensembles in Shear: Implications for Parameterization

CHANGHAI LIU AND MITCHELL W. MONCRIEFF

National Center for Atmospheric Research, Boulder, Colorado*

(Manuscript received 12 June 2000, in final form 15 December 2000)

ABSTRACT

A systematic numerical investigation is conducted into the role of ambient shear on the macrophysical properties of tropical cumulus ensembles maintained by convective available potential energy generated by constant surface fluxes of temperature and moisture and large-scale advective cooling and moistening. The effects of five distinct idealized wind profiles on the organization of convection, and quantities relevant to the parameterization of convection and convectively generated clouds, are examined in a series of 6-day two-dimensional cloud-resolving simulations.

Lower-tropospheric shear affects the mesoscale organization of convection through interaction with evaporatively driven downdraft outflows (convective triggering), while shear in mid-to-upper levels determines the amount of stratiform cloud and whether the convective transport of momentum is upgradient or downgradient.

Shear significantly affects the convective heating and drying, momentum transport, mass fluxes, and cloud fraction. Sensitivity is strongest in weaker forcing. Cloud-interactive radiation has little direct effect on a 6-day timescale. In particular, the effects of shear on convective momentum transport and cloud fraction are large enough to be potentially significant when included in parameterizations for climate models.

1. Introduction

It is well known that the transports of heat, moisture, and momentum by cumulus ensembles, and the radiative effects of convectively generated clouds, are key quantities that must be parameterized in general circulation models. However, present parameterizations do not take environmental shear into account. Shear has a marked effect on precipitating convection because it organizes the airflow into coherent structures on spatial scales from a few kilometers to thousands of kilometers, the full range of mesoscale motion. The association of shear with convective organization has long been recognized, for example, in the context of severe convective storms, squall lines, mesoscale convective systems, tropical cloud clusters, trade cumulus, and a diversity of convective regimes in polar outbreaks behind midlatitude cyclones (see Ludlam 1980; Cotton and Anthes 1989; Houze 1993 for background). Relationships between shear and convective organization have a rigorous theoretical basis in the nonlinear models of organized convection formulated by Moncrieff (1981).

The large-scale role of convective organization and its incorporation into parameterizations are potentially important for several reasons. First, convective organization is poorly understood in the context of the atmospheric water and energy cycles. Second, uncertainties in radiative transfer stemming from variability in vapor and condensate, while arguably acceptable in short-range numerical weather prediction, have marked repercussions in climate models. Cloud parameterization accuracy requirements are much more stringent for climate prediction than for weather prediction. While a systematic bias of 10% in cloud fraction could be tolerated in a weather forecast model, it would have unacceptable consequences in a climate model (GCSS 2000). Third, spaceborne profiling instruments within the next decade will provide an unprecedented range of cloud and precipitation measurements. The physical interpretation of those measurements requires a much improved understanding of cloud systems and how they interact with other scales of motion. Fourth, the resolution of state-of-the-art global numerical prediction models (presently about 50 km) will soon be about 10 km, capable of treating the larger mesoscale circulations explicitly.

In the latter context, we remark on the issue of scale separation (i.e., the assumption of a spectral gap between the scales being predicted and those being parameterized). It was shown long ago in the Global Atmosphere Research Programme (GARP) Atlantic Tropical Experiment (GATE), conducted in 1974, that convective rainfall and the attendant transports are manifestly mesoscale (Houze and Betts 1981). This as-

*The National Center for Atmospheric Research is sponsored by the National Science Foundation.

Corresponding author address: Dr. Changhai Liu, National Center for Atmospheric Research, P.O. Box 3000, Boulder, CO 80307-3000. E-mail: chliu@ucar.edu

pect is in conflict with the concept of scale separation. It is already an issue in global numerical weather prediction models and a vintage unsolved problem in regional models (Molinari and Dudek 1986; Zhang et al. 1988). Moncrieff and Klinker (1997) demonstrated that surrogate tropical superclusters, essentially the product of inadequate horizontal resolution, incorrectly process water and cause uncertainties in latent heating, evaporation, and dynamics.

Our paper is organized as follows. The next section describes the numerical model and experimental design, followed by the effects of shear on mesoscale organization in section 3. Aspects pertinent to parameterization are reported in section 4, and we conclude in section 5.

2. Design of the numerical experiments

We use the two-dimensional Eulerian version of the three-dimensional nonhydrostatic, Eulerian, semi-Lagrangian, anelastic model (Smolarkiewicz and Margolin 1997) at a resolution sufficient to resolve mesoscale circulations. The computational domain is 800 km wide and 30 km deep, with a 2-km horizontal and a 0.3-km vertical grid length. Free-slip boundary conditions are employed at the top and bottom of the domain, and periodic conditions at the lateral boundaries.

Microphysical processes are represented by a bulk two-category warm-rain parameterization (Grabowski and Smolarkiewicz 1996) and a bulk two-category ice parameterization (Grabowski 1999). The radiative transfer parameterization scheme of the National Center for Atmospheric Research Community Climate Model (Kiehl et al. 1994) is activated every 2 min (12 time steps). Instantaneous quantities, including temperature, water vapor mixing ratio, cloud water, and ice and snow mixing ratio, are used for the radiation code. The effective radius for liquid water is assumed to be 10 μm, whereas for ice particles the effective radius is a function of ice and snow content (McFarquhar and Heymsfield 1997).

In our simulations convective available potential energy (CAPE) is generated continuously by (i) constant surface sensible and latent heat fluxes of 30 and 150 W m^{-2}, respectively; and (ii) time-invariant, horizontally homogeneous large-scale advection of temperature and moisture that, for convenience, we call large-scale forcing. Two scenarios are investigated. The first, labeled ''S'' in Figs. 1a and 1b, represents strong large-scale forcing based upon the average over the Intensive Flux Array during the convectively active 19–26 December 1992 period of the Tropical Ocean Global Atmosphere (TOGA) Coupled Ocean–Atmosphere Response Experiment (COARE). The second, labeled ''W,'' has an identical shape but is half the magnitude of S. This is an idealization of the slowly varying forcing and shear in the real atmosphere.

We examine the effects of five idealized wind profiles (Fig. 1c) on convective organization and attendant properties: a motionless state (U0), constant flow (U1), shear

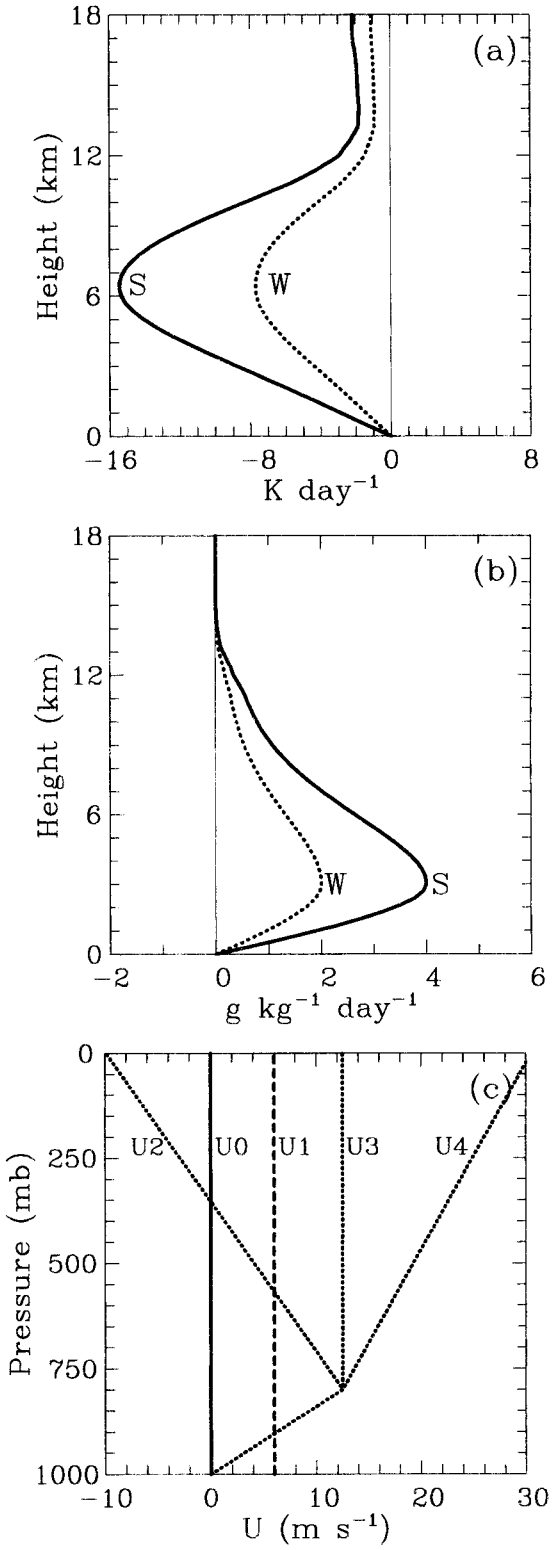

FIG. 1. (a) Potential temperature forcing (K day^{-1}), (b) water vapor forcing (g kg^{-1} day^{-1}), and (c) large-scale wind.

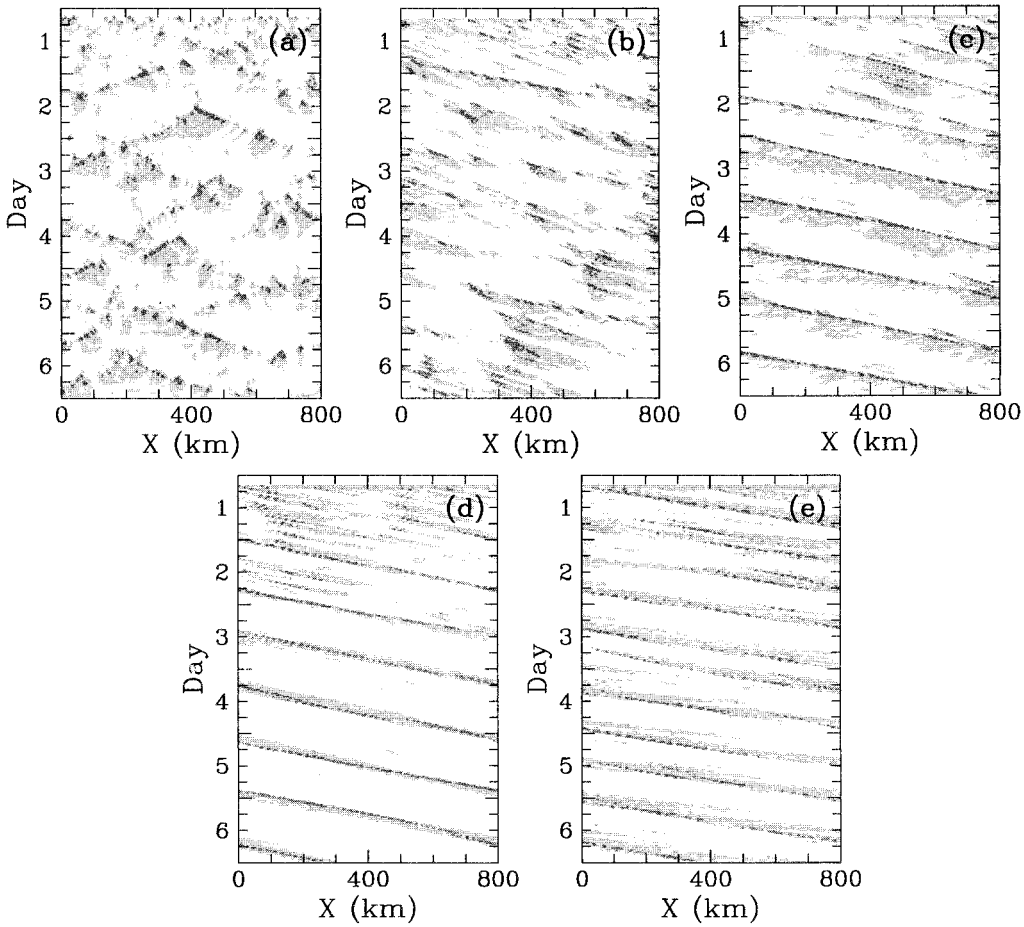

FIG. 2. Time–space plot of the precipitation rate in simulations with strong forcing. (a), (b), (c), (d), and (e) correspond to the wind profiles U0, U1, U2, U3, and U4, respectively, in Fig. 1c. The light and dark shading show precipitation rate larger than 1 and 10 mm h^{-1}, respectively.

reversal or jetlike flow (U2), shallow shear (U3), and deep unidirectional shear (U4). In order to maintain the wind profiles in a simple way, a relaxation term $(U - \overline{u})/\tau$ (where $\tau = 2$ h) is added to the right-hand side of the horizontal momentum equation. Here $\overline{u}(z, t)$ and $U(z)$ are the domain-averaged simulated horizontal wind component and the aforementioned profiles, respectively.

We conducted a total of fifteen 6-day numerical experiments consisting of three groups of five experiments, each corresponding to one of the above wind profiles, and incorporating strong forcing without cloud-interactive radiation, weak forcing without cloud-interactive radiation, and strong forcing with cloud-interactive radiation.

3. Effects of shear on mesoscale organization

The space–time distribution of the surface precipitation rate in Fig. 2 illustrates the organizing role of environmental shear. On average, convection is shorter lived in the unsheared environments (U0 and U1) but it is not randomly distributed, apart from the model spinup during the first few hours. As expected, cloud systems are more persistent and coherent in the sheared environments. In jetlike flow (U2), the convective system is characterized by a narrow region of intense precipitation trailed by extensive light precipitation (Fig. 2c). Because of the strong rearward airflow relative to the system translation, the condensate field (not shown) has a widespread trailing stratiform region but there is no forward anvil. This is a classic propagating squall line regime associated with shear reversal.

The effect of shear (especially upper-level shear) is manifested by convective organization and, especially, the *system relative flow*. In shallow shear (U3) the small upper-level relative flow prohibits both extensive trailing stratiform regions and leading anvils. Consequently, the surface precipitation is restricted to a narrow region (Fig. 2d). In deep shear (U4), the system has a forward anvil but no trailing stratiform region occurs because of the strong upper-level rear-to-front relative flow. Intense localized precipitation is led by extensive light precipitation (Fig. 2e), in direct contrast to the jetlike flow case. Convective systems and precipitation patterns

broadly similar to our numerically simulated systems have been identified in radar observations (Parker and Johnson 2000).

Our physical explanation for the mesoscale organization is based on the dynamics of density currents, together with the dynamics of organized convection in shear. For dynamical background, the reader is referred to Liu and Moncrieff (1996), Moncrieff and Liu (1999), and Moncrieff (1981, 1992). Density currents, surface pools of cold (dense) air produced by convective downdrafts, are an important mechanism for the continuous regeneration of convection, as in our simulations. They can also propagate great distances from their origin and trigger convection remotely in favorable environments. A density current propagates by virtue of the pressure gradient between the cold air and the ambient boundary layer. The propagation speed of a density current relative to the surface wind is $c - U_s = \sqrt{2\Delta p_s/\rho_s}$, where Δp_s is the surface pressure jump at the density current front, U_s the surface wind speed, and ρ_s the density. Because pressure is nonhydrostatic on small scales, dynamics partly determines Δp_s.

When the mean flow is zero (U0), the density currents generated by evaporatively cooled downdrafts, on average, spread out symmetrically leftward (westward) and rightward (eastward) of the initial convection. The forced ascent at each density current front triggers new convection. This growth cycle repeats and the convective activity progressively moves outward from the original convection, explaining the distinctive inverted v-shaped precipitation pattern in Fig. 2a.

Two distinct (slow moving and fast moving) regimes of organization are identified in Fig. 2b (where $c \approx 6$ and 12 m s^{-1}, respectively). The slower movement is consistent with the retarding effect of the headwind (U1), and the fast movement with the converse effect of a tailwind, on density current propagation. (Note that U1 = 6 m s^{-1} is strong enough to make the density current move eastward relative to the earth.) In a headwind, the density current front is deeper than average and an effective trigger, but the attendant strong airflow above the current steers incipient convection away from where it is initiated. This reduces the intensity and lifetime of the convection (see Fig. 5b of Moncrieff and Liu 1999). The slow-moving, short-lived regime is abundant throughout the simulation (Fig. 2b). On the other hand, the density current is shallower and the overlying airflow is slower in a tailwind, so the incipient convection tends to remain in proximity of the triggering. The fast-moving regime occurs between days 1.25 and 2 and traverses the computational domain, and a shorter-lived episode starts on day 5. Note that the westerly steering flow promotes eastward-moving systems with leading anvils.

In shear flow (profiles U2, U3, U4) highly organized, long-lived, eastward-moving mesoscale systems are prominent (Figs. 2c,d,e). Because the low-level shear is identical in each profile, differences among the simulated cloud systems are due solely to the upper-level shear. Low-level shear causes an overturning flow ahead of the density current instead of the typical up-and-over airflow in unsheared flow. Not only does the overturning provide forced lifting, it also anchors the incipient convection to this very effective trigger (Moncrieff and Liu 1999, their Fig. 1).

Deep unidirectional shear is not conducive to vigorous convection because the updrafts slope downshear; therefore, evaporation and loading of precipitation from the leading anvil decrease the buoyancy of the updraft inflow. In contrast, jetlike flow moistens (often to saturation) the mid- to upper tropophere. This results in extensive stratiform cloudiness associated with the deep rearward relative flow. Precipitation loading and evaporation do not inhibit the updraft in this scenario but, rather, enhance the mesoscale downdraft. These basic structural properties are explained by nonlinear dynamical models of organized convection in shear (Moncrieff 1981) and their archetypal forms (Moncrieff 1992). Specifically, the trailing anvil regime (U2), the leading and trailing anvil regime (U3), and the prominent forward-anvil/weak trailing anvil regime (U4) are consistent with the three relative flow patterns shown in Fig. 2 of Moncrieff (1992) (i.e., corresponding to $h_0 = 1$, 1/2, and 1/3, respectively).

Halving the advective forcing weakens the convection (not shown) because of the slower rate of generation of CAPE. The organization is otherwise similar to that in strong forcing. For example, the shear-free flows are characterized by intermittent convection, whereas shear flows produce organized, long-lasting regimes. The convection in the deep positively sheared flow is comparatively more sensitive to the large-scale forcing and not as long lasting.

4. Effects of shear on quantities relevant to parameterization

a. Thermodynamic budgets

Because the dynamical scales of cumulus ensembles are much smaller than resolvable by a rawinsonde network, the collective effects of convection are diagnosed indirectly, yielding the heat source (Q_1) and moisture sink (Q_2) of Yanai et al. (1973). On the other hand, these quantities can be calculated *directly* from cloud-resolving models using the relationships

$$\overline{Q}_1 - \overline{Q}_R = \frac{L_v}{c_p}(\overline{c} - \overline{c}) + \frac{L_s}{c_p}(\overline{d} - \overline{s}) + \frac{L_f}{c_p}(\overline{f} - \overline{m}) - \frac{\overline{\pi}}{\overline{\rho}}\frac{\partial}{\partial z}(\overline{\rho w' \theta'}) + \frac{\overline{\pi}}{\overline{\rho}}\frac{\partial \overline{F}_\theta}{\partial z} \quad (1)$$

$$\overline{Q}_2 = \frac{L_v}{c_p}(\overline{c} - \overline{e} + \overline{d} - \overline{s}) + \frac{L_v}{c_p}\frac{1}{\overline{\rho}}\frac{\partial}{\partial z}(\overline{\rho w' q_v'}) - \frac{L_v}{c_p}\frac{1}{\rho}\frac{\partial \overline{F}_{q_v}}{\partial z}. \quad (2)$$

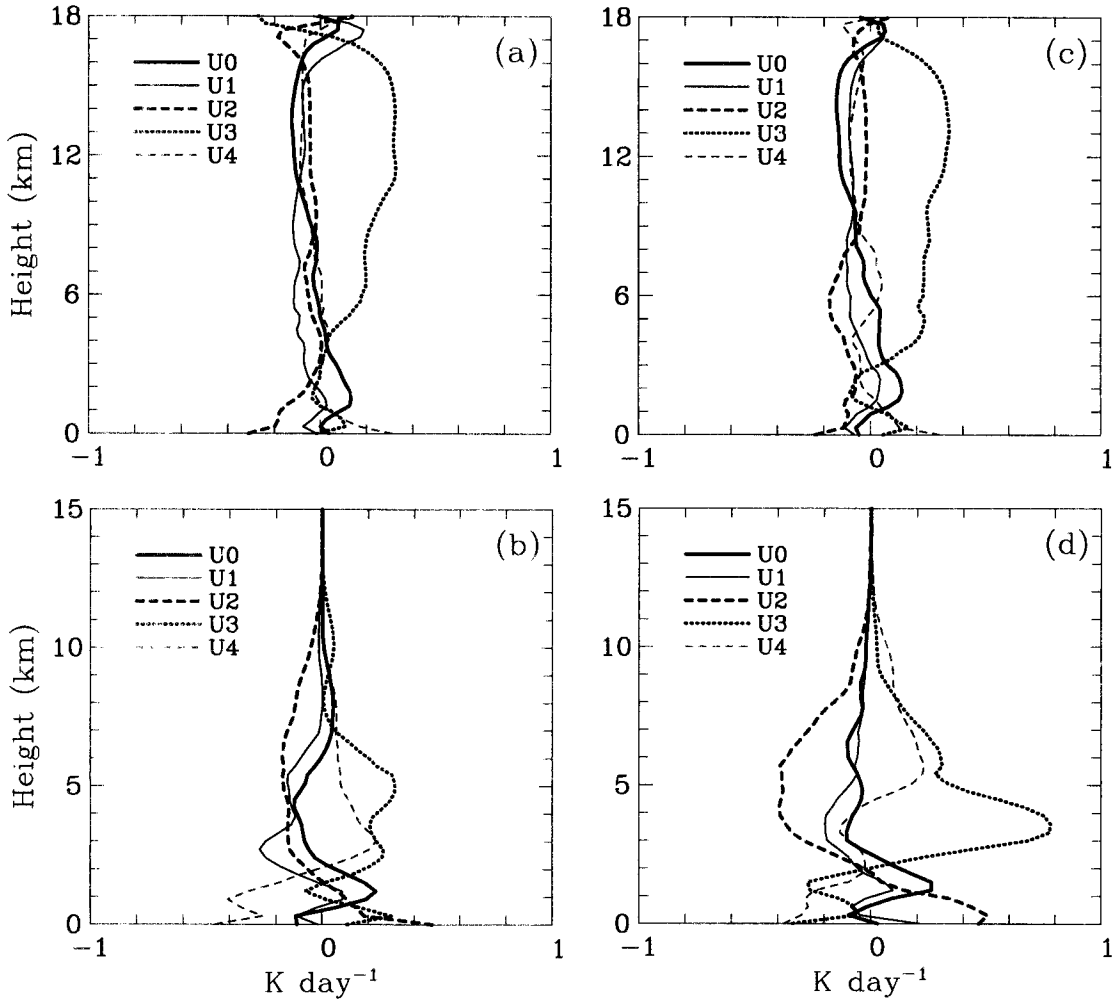

FIG. 3. Domain and time averaged profiles of (a) apparent heat deviations and (b) apparent moisture deviations from the respective mean in the five simulations with strong large-scale forcing. (c) and (d) The corresponding quantities for weak forcing.

The overbar represents the horizontal average, and the prime the deviation from the average; π the Exner function; Q_R the radiative cooling or heating; F_θ and F_{q_v} the subgrid flux of θ and q_v, respectively; c, e, f, m, d, and s the condensation, evaporation, freezing, melting, deposition, and sublimation rates, respectively; and c_p, L_v, L_f, and L_s the specific heat of dry air at constant pressure, the latent heat of condensation, latent heat of fusion, and latent heat of sublimation, respectively.

The convectively generated heating (drying) is similar among the simulations with the same forcing and is almost canceled by the imposed cooling (moistening), which is typical of the tropical atmosphere. In order to quantify the variability, the heat and moisture source deviations relative to their respective means in each group of simulations are presented. Figures 3a and 3b displays the results in simulations with the strong forcing but without cloud–radiation interaction. The difference in the heating is less than 0.5 K day^{-1}. While only a small fraction of the heat source, this is significant considering that the typical temperature tendency in the Tropics is on the order of 0.1 K day^{-1}. A similar argument applies to the moistening profiles. Considering the heat and moisture deviations, the shallow shear produces a warm and dry atmosphere at most levels. A cold and moist (warm and dry) planetary boundary layer occurs in jetlike flow (deep shear).

The conclusions from Figs. 3a and 3b are little affected by cloud-interactive radiation (not shown). First, the difference between the shallow sheared case and the others is smaller (greater) in heating (moistening) compared to the noninteractive radiation results. Second, the difference between the jetlike flow and the deep shear cases is larger in terms of heating but smaller in moistening at most levels. Third, the larger moistening occurs in motionless mean flow in the radiation-free simulations but in uniform flow with interactive radiation. Radiative feedback can either strengthen or deplete the

effects of shear on the convective heating and moistening. Note that the heating consists of contributions from radiation, latent heating, and eddy and subgrid transport that individually have significant variability but a much smaller combined effect.

The effects of shear on heating and moistening are explained as follows. The weak relative flow in upper levels limits the advection of convectively generated condensate into the environment and subdues the diabatic cooling and moistening due to evaporation, sublimation, and melting. These processes account for the strong heating/drying and generate the warm and dry regime in shallow shear.

The budgets for the weak forcing shown in Figs. 3c,d are remarkably similar to those in strong forcing except that the variability in moistening among the various cases is larger, implying that the effects of shear are enhanced by weak forcing.

b. Temperature and moisture perturbations

Figures 4a–c show the temperature and water vapor mixing ratio perturbations from the initial state and relative humidity profiles averaged over the domain throughout the 6-day integration for strong forcing. The marked similarity of the two unsheared cases confirms that uniform flow has a negligible impact because the fields are Galilean invariant and the effect of mean flow on the surface fluxes is excluded. In contrast, there is a strong sensitivity to shear. Within the mid- and upper troposphere above 2 km there is a prominent warm and dry regime in shallow shear, a relatively cold regime in deep shear, and a moist regime in jetlike flow. In the lowest 2 km a warm and moist state (in terms of water vapor mixing ratio) occurs in deep shear and a cold and dry state in jetlike flow. The temperature difference between the warm and cold profiles exceeds 2 K in the upper troposphere and near the surface.

The water vapor mixing ratio difference between the moist and dry profiles has a double peak, one in the midtroposphere and another near the surface. In terms of relative humidity, the moistest and driest atmospheres occur in the jetlike flow and shallow shear, respectively. The difference reaches 15%–20% in the 4–12-km layer.

Comparison with Figs. 4d–f shows that halving the advective forcing strength does not much affect the thermodynamic variability associated with the various wind profiles, such as the warm and dry regime in the shallow shear, the relatively cold regime in the deep shear, and the moist regime in jetlike flow.

Cloud-interactive radiation causes a net cooling so the domain-mean temperature is colder (not shown) and the water vapor mixing ratio is slightly reduced. Thermodynamic variability is broadly comparable, although in quantitative terms it is somewhat smaller (e.g., relative humidity) then in the radiation-free experiments.

c. Cloud fraction

Fractional cloudiness (cloud fraction) is parameterized in large-scale models, yet our physical understanding of what determines cloud amount is inadequate. In prognostic approaches, the representation of convectively generated clouds depends on detrainment of moisture provided by the convective parameterization. Detrainment is strongly affected by shear; for example, the generation of upper-tropospheric stratiform cloud and cirrus is a product of shear-induced dynamical organization, especially the front-to-rear outflow in jetlike shear.

The profiles of cloud fraction and total condensate (sum of cloud water, rainwater and ice mixing ratio) are displayed in Figs. 5a and 5b. In calculating cloud fraction, 100% cloudiness is assumed over a grid box when the condensate exceeds 0.01 g kg^{-1}. As in the thermodynamic fields, the difference between the two unsheared cases is minor except for somewhat less cloudiness in the zero mean flow. The condensate distributions in the three sheared cases are similar, apart from the relatively large amount of upper-tropospheric condensate in shallow shear. In contrast, the cloud fraction strongly depends on the relative flow, that is, on the shear-induced mesoscale organization. The relative flow generates widespread cirrus and advects convectively generated condensate either backward or forward, depending on the ambient shear. The greatest cloudiness (by a factor of about 2) occurs in the 5–12-km layer for jetlike flow. The least cloudiness occurs in shallow shear, despite the total condensate content being largest. The uniform distribution in shallow shear is consistent with the prevalence of upright convection, whereas the irregular pattern in the other scenarios indicate extensive anvils or stratiform regions. These results are consistent with the precipitation distributions shown in Fig. 2.

As indicated in Figs. 5c and 5d, the spatially and temporally averaged condensate and cloud fraction are much smaller (but reduced by less than 50%) when the large-scale forcing is halved. As in the thermodynamic fields, the effects of shear are largely independent of the forcing strength; for instance, both strong and weak forcing cause the greatest cloudiness in jetlike flow and the least cloudiness in shallow shear.

Interactive radiation slightly increases the condensate at most levels except in shallow shear. Because the shear dependence decreases, differences among the various flows are less noticeable. The cloud-radiative interaction affects positive feedback in that it increases the fractional cloudiness. Similar to the thermodynamic and condensate fields, the cloudiness variation in the various sheared environments is smaller but, for the most part, independent of radiative effects. The largest cloud fraction occurs in jetlike flow and the smallest in shallow shear, regardless of the influence of radiation.

Some large-scale models still use diagnostic parameterizations where cloudiness is estimated empirically

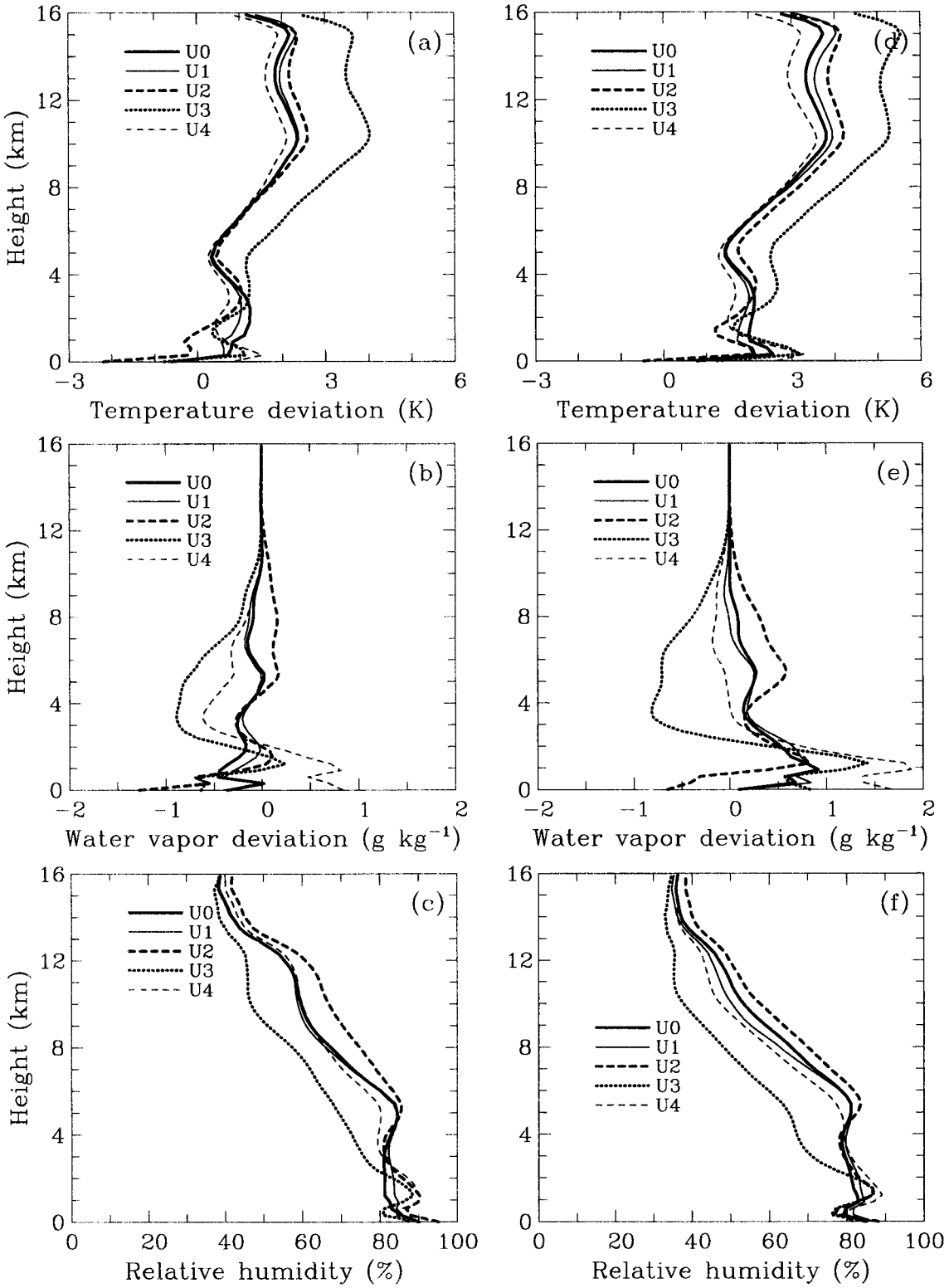

FIG. 4. Domain- and time-averaged profiles of (a) temperature deviation and (b) water vapor mixing ratio deviation relative to the initial state and (c) relative humidity in simulations with strong forcing. (d), (e), and (f) The corresponding quantities with weak forcing.

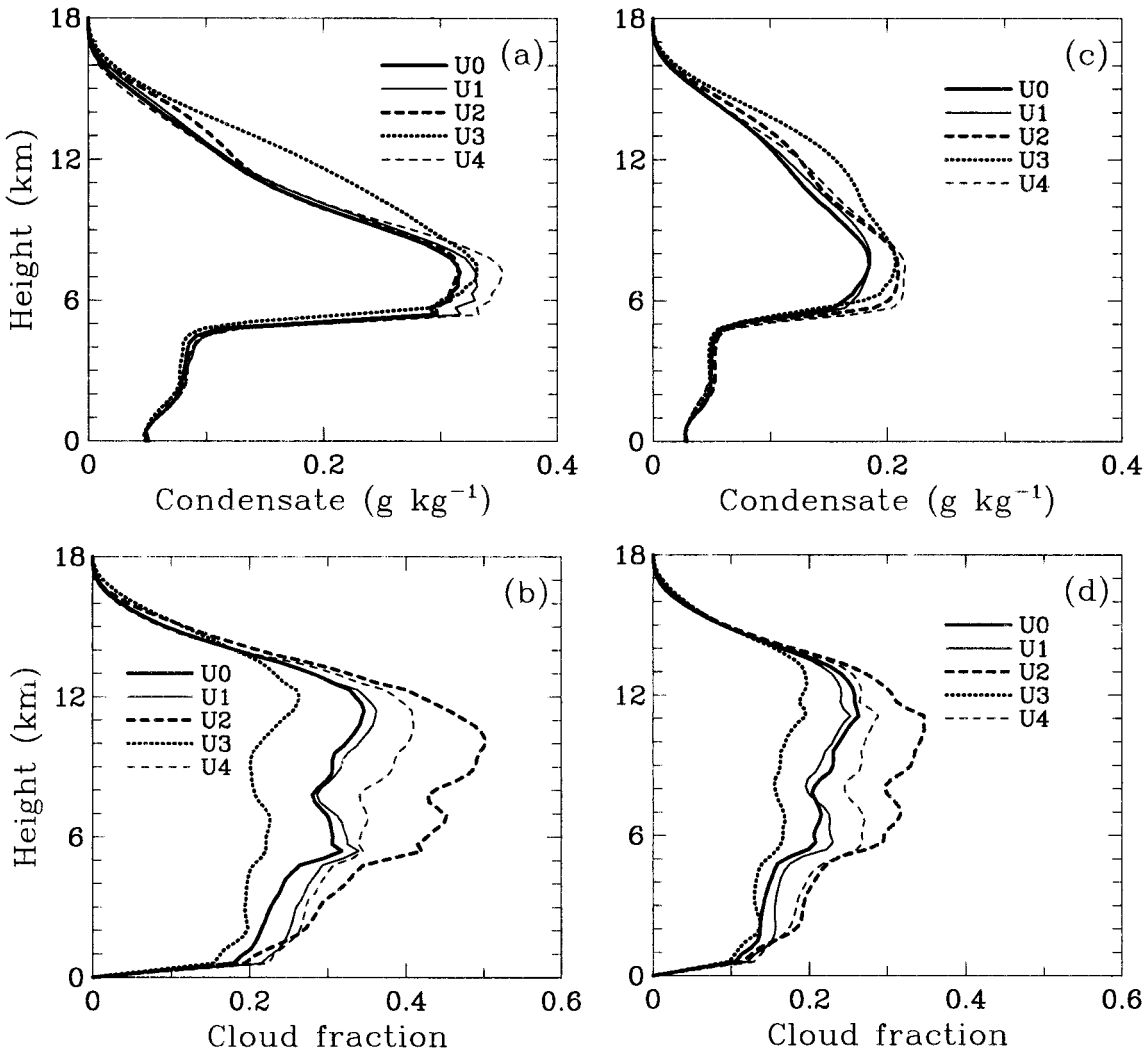

FIG. 5. Profiles of (a) total condensate and (b) cloud fraction averaged over the domain and the 6-day integration in simulations with strong forcing. (c) and (d) The corresponding quantities with weak forcing.

from large-scale variables. The relative humidity is the most frequently used quantity. When applied to the relative humidity in Figs. 4c and 4f, a diagnostic parameterization would produce the largest cloudiness in jetlike flow and the least in shallow shear, qualitatively in agreement with Figs. 5b and 5d. It would fail to represent the difference between deep shear and unsheared flows. Diagnostic parameterization could be improved by accounting for convectively generated stratiform cloud prevalent in shear flow.

d. Mass fluxes

The mass flux profiles in cloudy regions have a similar shape in all experiments, which is remarkable considering the different convective regimes. This likely reflects the constant forcing profiles prescribed throughout the 6-day simulations. In reality, the shape of the forcing, and therefore the vertical distribution of buoyancy and the location of maximum vertical velocity, will vary. However, note that systematic intercomparisons of cloud-resolving models show that convective mass flux has smaller variability than other quantities used in parameterization (Moncrieff et al. 1997).

Both upward and downward mass fluxes peak in the lower troposphere (Fig. 6a); as a rule, the larger the cloud fraction (Fig. 5b), the larger the mass flux. The mass fluxes in updraft and downdraft cores (defined when the absolute value of vertical velocity exceeds 1 m s^{-1} in the cloudy region) have more marked low-level extrema (Fig. 6b). The vertical distribution of mass fluxes in updrafts suggests strong detrainment around 6–9 km and abundant convection of intermediate depth (cumulus congestus) in addition to deeply penetrative cumulonimbus. Jetlike flow produces more midlevel detrainment than the other ambient flows. Shallow shear is associated with stronger convection.

The mass-weighted relative humidity in downdrafts

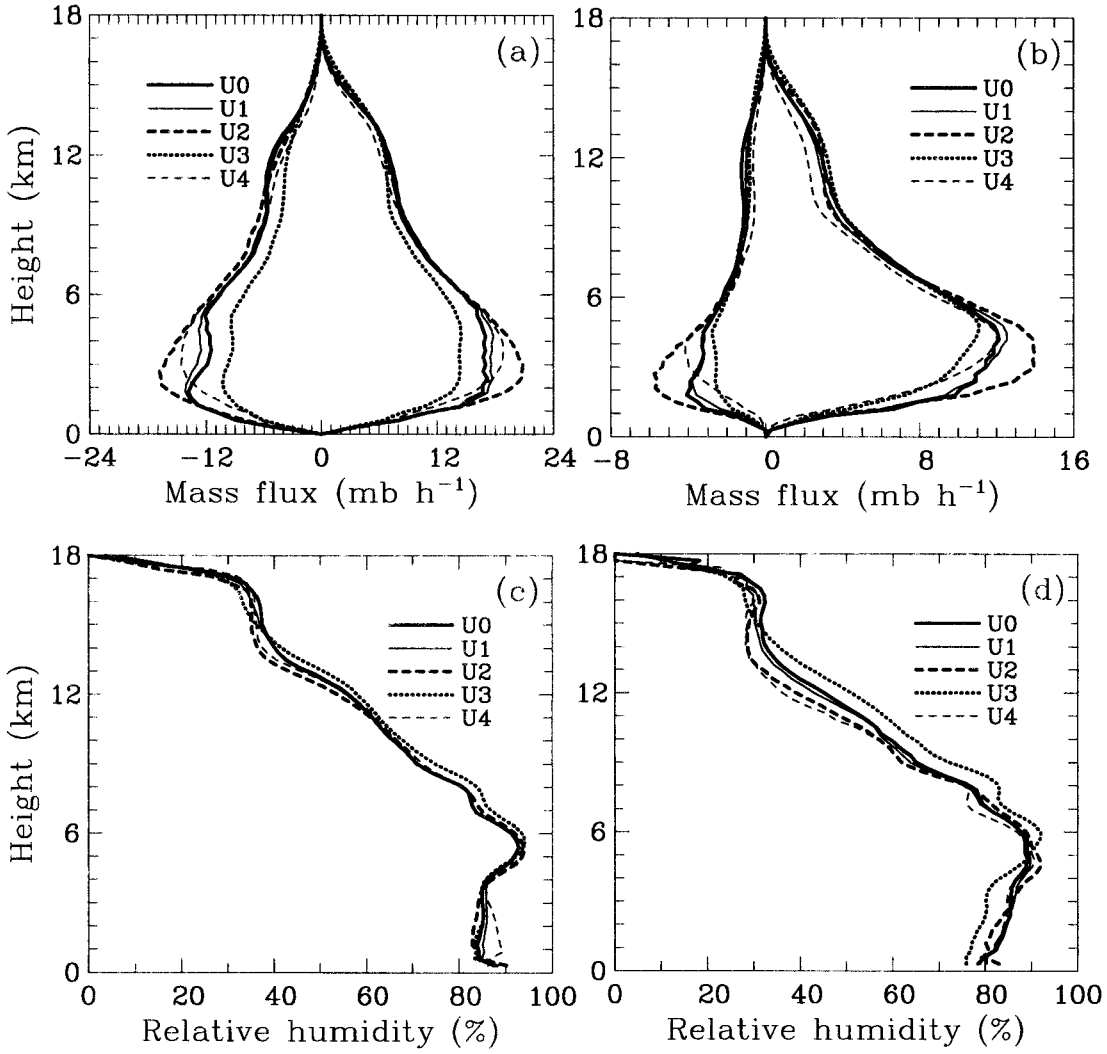

FIG. 6. Domain- and time-averaged profiles of updraft and downdraft mass fluxes over (a) cloudy region and (b) convective cores, and relative humidity in downdrafts over (c) cloudy region and (d) convective cores for simulations with strong forcing. Cloudy region is defined as having the condensate exceeding 0.01 g kg^{-1}, and convective core is defined as having the absolute value of vertical velocity exceeding 1 m s^{-1} in the cloudy region.

(Figs. 6c and 6d) is not sensitive to ambient flow and shear. The downdraft in the entire troposphere is subsaturated and, furthermore, downdraft cores are slightly drier than the weak descending airflow. The relative humidity in downdrafts is not necessarily correlated with the ambient relative humidity.

e. Momentum transport

The vertical transport of horizontal momentum is a strong function of the convective organization and therefore shear. Figure 7a shows the profiles of the time- and domain-averaged momentum fluxes ($\overline{\rho u' w'}$) in the simulations with strong forcing, where u' and w' are the horizontal and vertical velocity perturbations from the domain average, respectively. As expected, the momentum transport is negligible when the mean flow is zero (U0). It is small but not negligible in constant flow (U1), where the positive momentum flux in the lowermost 5 km is associated with weak, eastward-moving, leading anvil systems. These systems, products of nonlinearity associated with density-current triggering (see section 3), generate positive vorticity that accelerates the mean flow.

The sign and magnitude of the low-level shear compared to upper-level shear has a marked effect on momentum transport. In deep unidirectional shear (U4) the momentum flux is positive (i.e., upgradient), consistent with downshear-sloping airflow and the Moncrieff (1981) steering-level regime. The momentum flux is negative when there is shear reversal (U2), or when the upper-level shear is zero (U3). A negative flux is characteristic of an organized system traveling in the positive x direction and having a dominant front-to-rear

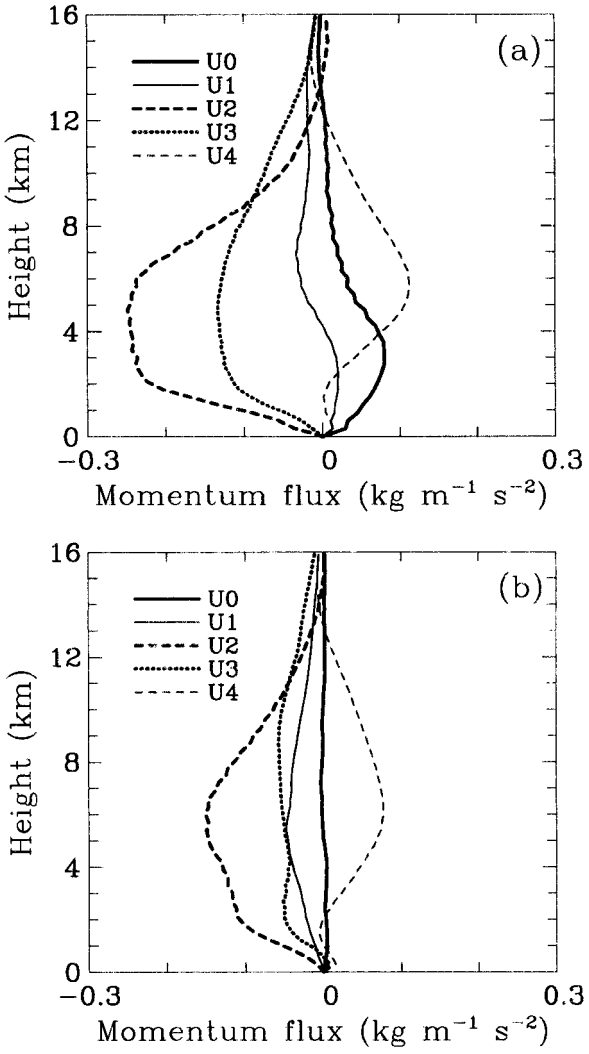

FIG. 7. Domain- and time-averaged profiles of momentum fluxes ($\overline{\rho u' w'}$) in simulations with (a) strong forcing and (b) weak forcing.

updraft. As a rule, momentum transport in jetlike flow and shallow shear has sign opposite to the direction of travel of the attendant convective system. In other words, the strength and sign of the upper-level shear compared to the low-level shear affect the basic nature of the convective momentum transport.

The momentum transport is explained by the analytic models of Moncrieff (1981, 1992). In particular, for the systems occurring in the U2 and U3 wind profiles, the negative sign of the momentum flux is opposite to the direction of propagation of the convective system because the updrafts slope upshear (see Figs. 5 and 10a of Moncrieff 1992). In deep positive shear the momentum flux has the opposite (positive) sign because of the attendant downshear tilt (see Fig. 10b of Moncrieff 1992). Note that upgradient and downgradient transport can occur simultaneously in different layers.

Figure 7b shows that weaker forcing affects the amplitude of the momentum flux but not its shape. Cloud-interactive radiation has little impact (not shown).

5. Conclusions

The effects of shear on cumulus ensembles, manifested through mesoscale organization, have received little attention in parameterization. In order to address this issue, we quantified the effects of shear on properties of cloud ensembles relevant to parameterization, such as convective heating and drying, momentum transport, and cloud fraction.

Convection is self-organized, albeit weakly, in unsheared flow due to continual triggering by downdraft outflow. The longest-lasting systems occur in shear for the following reasons. (i) Upper-level shear affects the extent of the stratiform region because it controls the morphology of the system-relative flow. (ii) A trailing stratiform region and a forward anvil develop in jetlike flow and in deep shear, respectively. (iii) Extensive stratiform regions (trailing or leading) tend not to occur in shallow shear. (iv) Low-level shear affects the convective triggering through the dynamical interaction of the low-level mean wind and shear with downdraft outflows. These aspects are explained by the dynamical modeling of density currents by Liu and Moncrieff (1996) and Moncrieff and Liu (1999).

Shear significantly affects convective heating and moistening. In particular, a warm and dry regime forms in the mid- and upper troposphere in the shallow sheared environment, a relatively cold regime in the deep positively sheared environment, and a moist regime in jetlike flow. At lower levels, a cold regime occurs in jetlike flow and a warm regime in deep shear. The maximum difference in the simulations is about 2 K in temperature, 2 g kg^{-1} in water vapor mixing ratio, and 20% in relative humidity. The difference in heating and moistening is, respectively, about 0.5 K day^{-1} and 0.5 g kg^{-1} day^{-1}, which is significant in the tropical atmosphere. The temperature and moisture deviations vary inversely with the strength of the large-scale forcing, indicating a marked nonlinearity (Fig. 4).

Shear strongly affects the convective momentum transport. Because momentum transport is a vector quantity, unlike the thermodynamic quantities, it is prone to three-dimensional effects. Strictly speaking, our two-dimensional modeling results are applicable to squall line–like mesoscale systems. While small in number, squall systems tend to be large in amplitude, for example, over continents during the warm season (notably west Africa), in easterly waves during GATE, and over the tropical oceans during the active phase of intraseasonal oscillations such as the westerly wind burst events observed in TOGA COARE. However, the contribution of squall line systems to the global momentum balance remains an open question. In order to address this question, systematic simulations of three-dimensional convection should be undertaken.

Convection in constant flow produces low-level positive momentum transport due to the nonlinearity of density current triggering. Organized convection in low-level shear produces coherent upgradient or downgradient transport in different layers. Upgradient transport occurs in deep shear. These characteristics are explained by the analytic models described in Moncrieff (1981, 1992).

Considering its variability in our simulations, the large-scale effects of convective momentum transport should be evaluated. Convective momentum transport is parameterized in some general circulation models, but its role is far from understood. The Lagrangian form of the horizontal momentum equation readily shows that the convectively generated pressure gradient is the key quantity, which is included in the Wu and Yanai (1994) and Gregory et al. (1997) parameterizations.

Our earlier comments on the relationship between triggering and shear need to be fully investigated considering that triggering is a major uncertainty in convective parameterization and, in particular, concerning organized convection.

Cloudiness generated by organized convection may prove to be the primary role of shear in a climate model. Cloud fraction is strongly modulated by upper-level shear. The stronger the system-relative upper-level wind, the larger the cloud fraction. The largest fraction (by about a factor of 2) occurs in jetlike flow and the smallest in shallow shear. In contrast to the temperature and moisture deviations, condensate and cloud fraction increase with the strength of the large-scale forcing. While shear has a marked effect on cloud fraction, it has comparatively little effect on the total amount of condensate. The significant variability of the cloud fraction (up to 40%) in our simulations implies that cloudiness variability due to shear is an important issue because, according to GCSS (2000), a systematic 10% uncertainty would be catastrophic in a climate model.

Finally, we conclude that momentum transport and cloud fraction, which are functionally related through the mesoscale dynamics of organized convection, are shear-dependent quantities that should be implemented in parameterizations in order to assess the impact of organized convection and attendant convectively generated clouds in climate models.

Acknowledgments. The National Center for Atmospheric Research is sponsored by the National Science Foundation. This work is supported by NASA TRMM Grant NAG5-7742.

REFERENCES

Cotton, W. R., and R. A. Anthes, 1989: *Storm and Cloud Dynamics.* International Geophysical Series, Vol. 44, Academic Press.

GCSS, 2000: *GEWEX Cloud System Study (GCSS). Second Science and Implementation Plan.* IGPO Publication Series, Vol. 34, 45 pp.

Grabowski, W. W., 1999: A parameterization of cloud microphysics for long-term cloud-resolving modeling of tropical convection. *Atmos. Res.,* **52,** 17–41.

——, and P. K. Smolarkiewicz, 1996: Two-time-level semi-Lagrangian modeling of precipitating clouds. *Mon. Wea. Rev.,* **124,** 487–497.

Gregory, D., R. Kershaw, and P. M. Inness, 1997: Parameterization of momentum transport by convection. Part II: Tests in single-column and general circulation models. *Quart. J. Roy. Meteor. Soc.,* **123,** 1153–1183.

Houze, R. A., Jr., 1993: *Cloud Dynamics.* International Geophysical Series, Vol. 53, Academic Press, 573 pp.

——, and A. K. Betts, 1981: Convection in GATE. *Rev. Geophys. Space Phys.,* **19,** 541–576.

Kiehl, J. T., J. J. Hack, and B. P. Briegleb, 1994: The simulated earth radiation budget of the National Center for Atmospheric Research community climate model CCM2 and comparisons with the earth radiation. *J. Geophys. Res.,* **99,** 20 815–20 827.

Liu, C., and M. W. Moncrieff, 1996: A numerical study of the effects of ambient flow and shear on density currents. *Mon. Wea. Rev.,* **124,** 2282–2303.

Ludlam, F. H., 1980: *Clouds and Storms: The Behavior and Effect of Water in the Atmosphere.* Pennsylvania State University Press, 405 pp.

McFarquhar, G. M., and A. J. Heymsfield, 1997: Parameterization of tropical cirrus ice crystal size distributions and implications for radiative transfer: Results from CEPEX. *J. Atmos. Sci.,* **54,** 2187–2200.

Molinari, J., and M. Dudek, 1986: Implicit versus explicit convective heating in numerical weather prediction models. *Mon. Wea. Rev.,* **114,** 1822–1831.

Moncrieff, M. W., 1981: A theory of organized steady convection and its transport properties. *Quart. J. Roy. Meteor. Soc.,* **107,** 29–50.

——, 1992: Organized convective systems: Archetypal dynamical models, mass and momentum flux theory, and parameterization. *Quart. J. Roy. Meteor. Soc.,* **118,** 29–50.

——, and E. Klinker, 1997: Mesoscale cloud systems in the tropical Western Pacific as a process in general circulation models. *Quart. J. Roy. Meteor. Soc.,* **123,** 805–827.

——, and C.-H. Liu, 1999: Convection initiation by density currents: Role of convergence, shear, and dynamical organization. *Mon. Wea. Rev.,* **127,** 2455–2464.

——, S. K. Krueger, D. Gregory, J.-L. Redelsperger, and W.-K. Tao, 1997: GEWEX Cloud System Study (GCSS) Working Group 4: Precipitating convective cloud systems. *Bull. Amer. Meteor. Soc.,* **78,** 831–845.

Parker, M. D., and R. H. Johnson, 2000: Organizational modes of midlatitude mesoscale convective systems. *Mon. Wea. Rev.,* **128,** 3413–3436.

Smolarkiewicz, P. K., and L. G. Margolin, 1997: On forward-in-time differencing for fluids: An Eulerian/Semi-Lagrangian non-hydrostatic model for stratified flows. *Atmos. Ocean Spec.,* **35,** 127–152.

Wu, X., and M. Yanai, 1994: Effect of vertical wind shear on the cumulus transport of momentum: Observations and parameterization. *J. Atmos. Sci.,* **51,** 1640–1660.

Yanai, M., S. K. Esbensen, and J.-H. Chu, 1973: Determination of the bulk properties of tropical cloud clusters from large-scale heat and moisture budgets. *J. Atmos. Sci.,* **30,** 611–627.

Zhang, D.-L., E.-Y. Hsie, and M. W. Moncrieff, 1988: A comparison of explicit and implicit predictions of convective and stratiform precipitating weather systems with a meso-β-scale numerical model. *Quart. J. Roy. Meteor. Soc.,* **114,** 31–60.